Available online at www.sciencedirect.com
ScienceDirect
ELSEVIER
Ultramicroscopy 107 (2007) 25–39
ultramicroscopy
www.elsevier.com/locate/ultramic

A procedure to analyze surface profiles of the protein molecules visualized by quick-freeze deep-etch replica electron microscopy

Yoshitaka Kimori[a,b], Yosuke Oguchi[c], Norihiko Ichise[d], Norio Baba[c], Eisaku Katayama[a,*]

[a]*Division of Biomolecular Imaging, Institute of Medical Science, The University of Tokyo, Minato-ku, Tokyo 108-8639, Japan*
[b]*Department of Bioscience and Bioinformatics, Kyushu Institute of Technology, Iizuka, Fukuoka 820-8502, Japan*
[c]*Department of Electric Engineering, Kogakuin University, Hachioji, Tokyo 192-0015, Japan*
[d]*Department of Visual Communication, Komazawa Women's University, Inagi, Tokyo 206-8511, Japan*

Received 6 October 2005; received in revised form 2 April 2006; accepted 12 April 2006

Abstract

Quick-freeze deep-etch replica electron microscopy gives high contrast snapshots of individual protein molecules under physiological conditions in vitro or in situ. The images show delicate internal pattern, possibly reflecting the rotary-shadowed surface profile of the molecule. As a step to build the new system for the "Structural analysis of single molecules", we propose a procedure to quantitatively characterize the structural property of individual molecules; e.g. conformational type and precise view-angle of the molecules, if the crystallographic structure of the target molecule is available. This paper presents a framework to determine the observed face of the protein molecule by analyzing the surface profile of individual molecules visualized in freeze-replica specimens. A comprehensive set of rotary-shadowed views of the protein molecule was artificially generated from the available atomic coordinates using light-rendering software. Exploiting new mathematical morphology-based image filter, characteristic features were extracted from each image and stored as template. Similar features were extracted from the true replica image and the most likely projection angle and the conformation of the observed particle were determined by quantitative comparison with a set of archived images. The performance and the robustness of the procedure were examined with myosin head structure in defined configuration for actual application.

PACS: 42.30.Sy; 68.37.Lp; 87.15.−v

Keywords: Quick-freeze deep-etch replica electron microscopy; Heavy meromyosin; Mathematical morphology; Pattern recognition

1. Introduction

Direct observation, measurement and manipulation of single protein molecules under functional conditions constitute the fundamental means of "single-molecule physiology" which should have been developed as the due course in the studies of biological motor-proteins [1]. Since biological molecular machines should work certainly in a stochastic manner, the absolute advantage of this methodological concept is obvious, enabling us to characterize various properties of single molecules in action without averaging. Thus, the innovating techniques as above were readily accepted as one of the most powerful experimental system tools in biophysics and cell-biology of various materials. Conventional methods of structural biology, such as X-ray crystallography and NMR analysis, collects the data from a vast number of purified molecules to give precise atomic coordinates after extensive averaging spatially and temporarily. Though expediently classified as a method of structural biology, electron microscopy (EM) occupies a unique position in terms that it can directly visualize the structure of individual molecules separately. Among various methods to prepare EM-specimen from the original biological macromolecules, ice-embedding by quick-freezing is naturally the most ideal technique to preserve the instantaneous structure of raw material without staining. Together with the powerful

*Corresponding author. Tel.: +81 3 5449 5512; fax: +81 3 5449 5419.
E-mail address: ekatayam@ims.u-tokyo.ac.jp (E. Katayama).

0304-3991/$ - see front matter © 2006 Elsevier B.V. All rights reserved.
doi:10.1016/j.ultramic.2006.04.012

"single-particle analysis" method, this cryo-EM technique have already taken an invaluable part to capture three-dimensional structure of large protein assembly [2–6]. In order to automatically pick up extremely low contrast images of protein particles from the background, various information theories were successfully applied to more reliable procedure [7,8] than before.

The most serious weakness of such near-ideal method, however, is the fragility of the protein molecule against the electron beam, which limits the dose of the available irradiation. To earn enough information for structural analyses, one should collect a huge number of images of highly purified protein molecules or supramolecular assemblies, classify their images according to the view angles (and sometimes the conformational difference), then take the average within each class. There, classification is the most crucial step for the success, sometimes resulting in different structures for the same molecule [9]. The situation is even more problematic if the target molecule is flexible and takes multiple or contiguous configurations, such as in the case for functioning motor-proteins. Each image might be too noisy for the unambiguous classification, and the essential structural information related to the function of molecular machines might be permanently lost if averaging is done in an inappropriate manner. Some method to visualize individual molecule with sufficient S/N ratio is the absolute requirement, just as the introduction of high-sensitivity fluorescence detector was previously so in single molecule physiology.

Quick-freeze deep-etch replica EM technique [10] might be one of the few strong candidates to satisfy such conditions. Since freeze-replica specimens consist of heavy metal and carbon, they are not only tolerant to extremely high electron dose, but also give highly contrasted images of single protein molecules that can be easily recognized even by inexperienced observers. Considering that the image contrast of this specimen is given in a similar manner to conventional low-angle rotary-shadowing, it might be natural to assume that the final images would be deteriorated by the granularity of platinum/carbon coating. However, the grain size of the freeze-replica image is extremely fine and is almost undetectable even by examination of highly magnified views of the original micrographs. Usukura et al. [11] noted that conventional rotary-shadowing can also give the images with substantially reduced grain-size, merely by shadowing performed at low temperature. This supports the view that granular appearance of the background by conventional shadowing at room temperature might be, at least partly, due to the movement of original fine metal particles to coagulate into large islets to deteriorate the apparent resolution [12]. Eskandari et al. [13] and Walz et al. [14] independently estimated that freeze-replica specimen includes the structural information up to 1 nm or even better, in accordance with our data. It was also shown by experimental and simulation studies, that rotary shadowing provides much more uniform metal coating [15] with higher resolution [12] than unidirectional shadowing. Thus, the spatial resolution of quick-freeze replica samples is certainly much higher than presumed from the granular impression of conventional low-angle shadowing.

By careful observation of such freeze-replicated images of the protein assembly, one could notice the presence of subtle light and dark gray-scale patterns on the surface of the individual molecules (Fig. 1(a), [16]). Considering that the image contrast due to heavy metal shadowing, it is easily supposed that the pattern might somehow reflect the surface profiles of the protein covered with thin metal deposit according to the incident beam angle of the metal vapor from distant evaporation source. When the particles like protein assembly were shadowed while rotating, the amount of the metal deposit at given position would be the function of the maximum inclination at that position along the surface of the target. The image contrast of nearly untilted views of the replicated specimen might arise mostly according to the density gradation projected onto the horizontal plane normal to the incident electron beam. Thus, the grooves and hills having less and more metal deposit would appear brighter and darker than the surrounding area, respectively. If the above assumption is correct, we might be able to determine the approximate view-angle of each single molecule in the EM field, together with the conformational type of the target, by comparison with appropriately surface-rendered atomic model. As a matter of fact, we realized empirically that the delicate surface pattern observed in freeze-replicated protein molecules could be surprisingly well-presented by a light-rendering software if the shadowing conditions were imitated as the illumination from multiple directions around the target molecules [17] (Fig. 1(b)). A rough orientation of a particle was defined by similarity comparison with a movable model image of the target by an interactive visualization tool, as the example shown in Figs. 1(c) and (d) (Katayama, unpublished result; see also Refs. [16,17]). We examined such recognition process by self-analysis and found that a human brain judges the identity of the image and the atomic model, not by a single-type feature but by multi-step procedure to discriminate different kinds of features at the same time. We reached the idea that the recognition of outline shape, together with a delicate pattern visible on the molecule's surface might be the essential steps of the identification process, that prompted us to incorporate these steps into computer-assisted recognition procedure. Our final goal is to establish the new methodology to automatically pick up the images of individual protein molecules, whether single or in complex, from replica EM field and precisely determine its conformational type and view angle, by comparison with the list of conformers registered in the data-base. Were the degree of matching not enough, we might be able to partly modify the atomic model for better matching. Along that way, the configuration of each protein molecule under various functional states could become within the reach of our analysis, if the proper

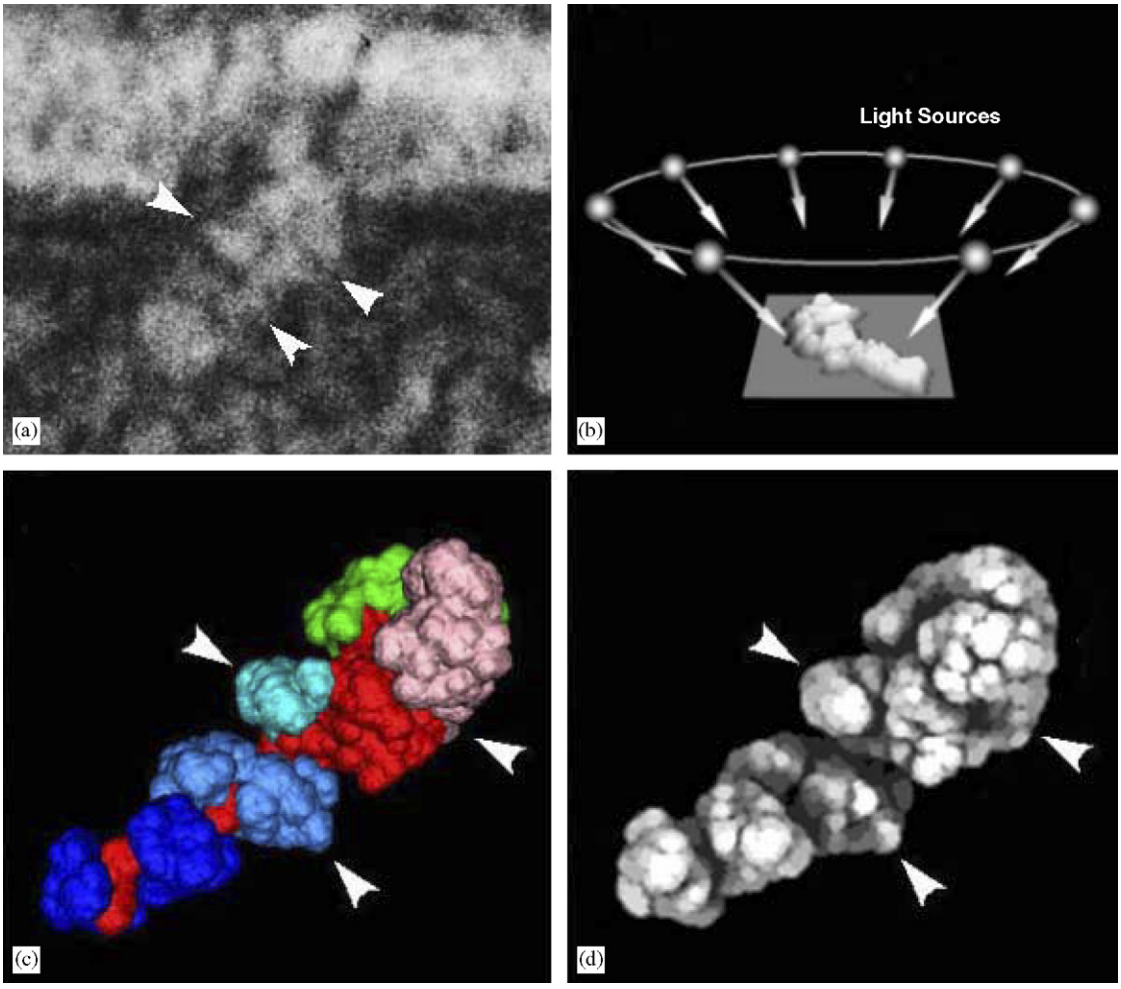

Fig. 1. (a) An example of quick-freeze deep-etch replica image of myosin head attached to actin-filament under rigor state. Note the presence of delicate pattern on the surface of the molecule. (b) Schematic presentation of the process to generate the template images by virtual lighting of the solid atomic model from eight directions. (c) Surface-rendered model image of most likely conformation (near-rigor state; 1DFK) and the view angle which were determined manually. The image was produced by homemade visualization tool, with subdomains represented in different colors. (d) The artificial image of 1DFK in the same solid angle as above but generated by virtual lighting. Corresponding landmarks in (a), (c) and (d) are indicated by arrowheads.

method to identify the surface feature of the molecules exists.

In this work, we present a novel algorithm dedicated to identify the Euler angle and the conformational type of given image of single molecule picked up from the field of quick-freeze replica specimens, taking heavy meromyosin head structure as an example.

2. Procedure for comparison of real and computer generated images

2.1. Main conception

In order to identify the surface feature of the replica image to the view from specific solid angle, we need to compare the real image with a comprehensive set of artificial images that possess the essential factors requested for the recognition of surface profile features. Since the purpose of our analysis is merely to define the configuration and the view-angle of the specific molecules visualized by shadowing, the outline shape and the position of prominent surface features that possibly correspond to subdomain arrangement are necessary and sufficient information to execute the following steps.

Fig. 2 shows a flow diagram of our image processing system that consists of two phases. In archiving phase, a comprehensive set of artificial images of the atomic model were generated as templates, from 3D coordinates of the protein molecule in question, by postulating its replica images viewed from all the directions. To efficiently prepare many artificial images, we employed commercial light-rendering program, as the easiest and the fastest way to collect the templates including the required structural information for comparison and matching. More specifically, a rotational series of images were produced to cover all the solid angles, assuming a virtual solid model of the protein molecule as illuminated by a number of surrounding light-sources from the appropriate elevation angles.

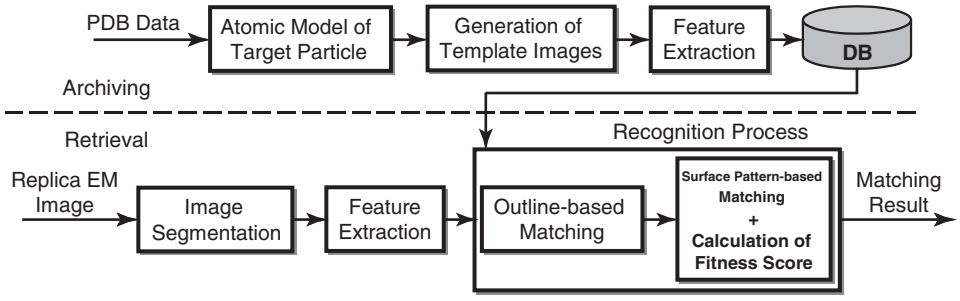

Fig. 2. Flow diagram of proposed procedure. See details in the text.

The outline shape and the surface profile pattern of the molecule were extracted from each template utilizing a new filter, as the characteristic features and then stored in the database, together with the area surrounded by the outline. In retrieval phase, true replica image was digitized and its contrast was reversed for comparison with the model images, because the metal-evaporated area appears darker than the carbon background (quick-freeze deep-etched images are conventionally presented after contrast reversal so that they look like natural objects softly illuminated by moonlight, to human eyes). The target particle was cropped from the field, and the same characteristic features as above were extracted in a similar manner. Because of different image-forming mechanism, the global appearances of real and artificial images were not close enough for the direct correlation analysis. So, they were pre-processed for texture-matching as described shortly.

The characteristic features of the target image were quantitatively compared with those of archived templates one by one, to finally determine its best-matched configuration and the orientation in 3D space. Actual examination was carried out in two steps, first by the outline, then, the surface feature pattern of the particles. At the same time, the fitness value of the selected molecule; the overlapping area of two kinds of images after fitting the respective patterns, was evaluated as the responsive score for the final decision.

Since the final aim of the present procedure is to determine the instantaneous structural states of given single protein molecules captured in freeze-replica images, we applied the same approach to assess the best-matching configuration for a given image as well, among the known conformers.

2.2. Theoretical basis and development of new image-processing filter

In conventional computer-assisted image processing, image signals including some periodical or symmetrical features are usually transformed to a sum of Fourier components as a convenient form for digital computation. Mathematical morphology is another approach more suitable for the detection of the size and orientation of the object, by taking the image as signals with various geometrical features. In the present work, we designed two kinds of filters based on mathematical morphology, one to segregate the target particle from the background in EM field and the other to extract protein molecule's surface pattern produced by shadowing the engraved relief profile, especially the subtle details that could not be readily recognized by non-expertise human eyes.

Below, the concepts of basic morphology operations and the morphological filter are described.

2.2.1. Basic morphology operations

Mathematical morphology is based on set-theory concepts of shape [18]. An image can be represented by a set of pixels. Morphological operations deal with two images always as a set: an objective image to be analyzed and a structuring element (SE), which is analogous to the kernel of a convolution operation. Each SE has a shape as a parameter of the operation. The shape of the SEs in these operators is chosen from either of square, circle, diamond, cross and line segment, etc. The shape and the size of SE play a crucial role in such type of processing and must be flexibly adapted to the geometric properties of the objects to be processed. A *flat* (binary) SE is the default for the morphological algorithm, because of the computational advantage. In smoothing process, it is more suitable than *non-flat* (gray-scale) SE to preserve some inter-region boundaries without blur. Hence, we concentrated on morphology using flat SEs throughout our processes.

The two basic morphological operations are dilation and erosion [19]. All other morphological operations are sequential combination of two basic operations; e.g. the two popular nonlinear filters are opening, an erosion followed by a dilation, and a closing, vise versa, respectively [20–25]. Haralick and colleagues [19] defined morphological operations as follows. Dilation and erosion are calculated as minimum and maximum value given in Eqs. (1) and (2), respectively. Here, the functions f and g are a gray-scale image and an SE, respectively.

Dilation:

$$(f \oplus g)(X) = \max_{X-Z \in F, Z \in G} \{f(X-Z) + g(Z)\}. \quad (1)$$

Erosion:

$$(f \ominus g)(X) = \min_{X+Z \in F, Z \in G} \{f(X+Z) - g(Z)\}. \quad (2)$$

F and G are the domains of f and g, respectively, satisfying f: $F \to E$, g: $G \to E$. E is a Euclidian space.

Opening:

$$f_g = (f \ominus g) \oplus g. \tag{3}$$

Closing:

$$f^g = (f \oplus g) \ominus g. \tag{4}$$

The opening operation eliminates upwardly convex parts smaller than the SE from the objective signal. On the contrary, the closing operation fills downwardly convex parts smaller than the SE. Accordingly, we see that the upwardly convex features of the objective signal are extracted by the difference between the original signal and the result of opening operation. Similarly, downwardly convex features of the objective signal are extracted by the closing operation.

2.2.2. Morphological smoothing filter

Image segmentation has been widely used [26,27] in EM to extract the target particles form the background. Its general algorithm is based on two properties; similarity and discontinuity, of gray-scale value. Since the segmentation of the region of interest (particle region) should be separated from the rest by the surrounding edge, the algorithm is to subdivide the image based on rapid changes in gray level across the periphery. So, pre-processing of the original image by smoothing is important. Appropriate segmentation requires the edge structure be preserved, and the brightness change to be smoothed within the particle region.

Median filter is commonly used for smoothing. Though it works effectively to remove shot or salt and pepper types of noise, while preserving the edges (perfect step edges), it degrades thin lines and features smaller than half the area of window size, and is not appropriate for dense noise removal. On the other hand, non-linear morphological smoothing filter is useful for noise reduction of gray-scale images corrupted by dense, low-amplitude, random or patterned noise [28]. Opening and closing are two operators commonly used to smooth the image in different ways. Opening can remove peaks (positive impulse), and closing can fill pits (negative impulse). In order to remove the positive and negative impulsive noise in certain images at the same time, opening and closing are usually used as a cascade. Maragos defined open-closing (OC) and close-opening (CO) filters using the same SE [21]. OC or CO filter gives better performance than median filter at removing noise while preserving the edges [29,30]. Stevenson and Arce [29] demonstrated from the statistic viewpoint, that the distribution of the output of the CO operator was biased toward higher values than the input distribution. The output distribution of OC was analogous to CO, but biased toward smaller values. Thus, smoothing by biased morphological operators may not be suitable to process the images where preservation of intensity levels is crucial. Since morphological operators are defined in complementary pairs which are equally and oppositely biased, one potential solution to the biasing problem is to average the complementary operators.

To achieve better smoothing, we employed a morphological smoothing filter called the LOCO filter [31] that is a linear combination of OC and CO. It was defined as follows:

$$\mathrm{LOCO}(f;g) = \frac{1}{2}(f_g)^g + \frac{1}{2}(f^g)_g. \tag{5}$$

LOCO(f;g) gives an approximate smoothing with respect to the SE and, unlike its constituent operators, is unbiased with respect to gray level.

2.2.3. Rotational mathematical morphology

Morphological filters; in particular, openings and closings, are superior to linear filters for smoothing, but has a common weak-point that a unique type of artifact might appear in the output, depending on the shape of the filter kernel (i.e. SE), due to remaining convolution effect of the SE shape. This artifact could invoke a serious problem in processing boundaries. In conventional mathematical morphology, the orientation of SE is fixed throughout the whole process, making the operation of the image with the complex directional features impossible. This artifact could influence the next recognition process. Thus, an outline along the boundary of a molecule region was used in this study, as one of the features to be recognized. In the ideal case, unnatural artifact might be relaxed, if a perfect circle SE can be used, but it is not practical to expect that a perfect circle is drawn as a discrete image, nor being expressed as a square if size of a SE becomes small, and line-segment SE might sometimes be necessary. Accordingly, we devised more universal technique to reduce this artifact and proposed a new smoothing method utilizing rotational mathematical morphology [32,33] to improve the extracting accuracy of the outline around the molecule region. In this strategy, multiple SEs rotated at an arbitrary angle were used with bicubic interpolation. This processing has the absolute advantage to suppress artifactual patterns, preserving the structural details, regardless of the direction of SE in the image.

We also propose the LOCO filter involving rotational mathematical morphology for Opening and Closing. This method utilizes a square or a disk shape as the structure element for smoothing. Assume that the straight angle (180°) is equally divided into N directions. Let g_i denote the rotation of a SE g by the degree of $180i/N$, where $i = 0, 1, \ldots, N-1$, and by let (k,l) denote 2D coordinates. In Refs. [34,35], multiple SEs were applied to the image and the maximum value among the opening operations was taken as the result at the coordinate in question. The maximum opening of f by g is defined as

$$Y_{\mathrm{op}}(k,l) = \max[Y_0(k,l), Y_1(k,l), \ldots, Y_{N-1}(k,l)], \tag{6}$$

where the image Y_i is the image f opened by g_i. In this operation, the SEs are floating freely under the surface of

an image, after the operation, and any part of the surface will be removed if none of these SEs fits under the surface. By the duality between opening and closing, the minimum closing can be described in a similar way. The minimum closing of f by g is defined as

$$Y_{\mathrm{cl}}(k,l) = \min[Y^0(k,l), Y^1(k,l), \ldots, Y^{N-1}(k,l)], \tag{7}$$

where the image Y^i is the image f closed by g_i. In this operation, the SEs are floating freely above the surface of an image, and any downward part of the surface will be filled in, if none of these SEs fits above the surface.

The results of smoothing by the proposed method (LOCO filter based on rotational mathematical morphology) were compared with those by conventional LOCO filter. It is notable that the internal structure and outline shape of the object were well preserved during noise reduction process. Fig. 3 shows an example of smoothing by a LOCO filter. The original image (Fig. 3(a), 123×123 pixels) has 8-bit gray-scale. The deteriorated image (Fig. 3(b)) was made by adding a random noise with the brightness from 0 through 255 to the original. Figs. 3(c) and (d) exhibit the results of smoothing with $n \times n$ square-shaped SEs of different size ($n = 5$, 9). Fig. 3(c) shows the result by conventional LOCO filter. More noises were removed by increasing the SE size, but the internal object of the circle and the diamond were deformed as influenced by the shape of SE. On the other hand, smoothing according to our proposal gave apparently the better result (Fig. 3(d); $N = 8$ for this case), considering the balance of the computer time and the performance. The structure of the object in the original image was well-preserved, even with the large size of SE.

The recovery from a noisy image was evaluated by normalized mean square error (NMSE) between a restored image ($\hat{f}$) of size $H \times W$ and the original image (f) of size $H \times W$, that was defined as

$$\mathrm{NMSE} = \frac{\sum_{i=1}^{H}\sum_{j=1}^{W}[f(i,j) - \hat{f}(i,j)]^2}{\sum_{i=1}^{H}\sum_{j=1}^{W} f^2(i,j)}, \tag{8}$$

where i and j are the row and column position within $\hat{f}$ and f. It is obvious from Fig. 3(e) that the proposed method is much better than the conventional ones in NMSE. Fig. 3(e) show the NMSE value of smoothing with $n \times n$ square-shaped SEs of different size ($n = 3$, 5, 7, 9, and 11 pixels). Our new method not only showed a superior performance to that of conventional one for all SE sizes but also was effective for SEs of various shapes.

2.2.4. Top-hat transform

We designed a top-hat transform filter to effectively extract delicate surface feature pattern of the target protein molecule, since the isolation of convex gray-scale objects can be accomplished by this kind of transform [36]. There, the opening operation was anti-extensive, in the sense that the gray level of every pixel in the opened image was not greater than that in the original image because the objects with high gray level having supports smaller than that of the SE should be eliminated by the opening operation. So, the residual of the opened image from the original image can be defined as top-hat transform (TH):

$$\mathrm{TH} = f - f_{\mathrm{g}}. \tag{9}$$

We succeeded to remove the artifact as above by the opening operation with the rotational mathematical morphology, Eq. (6).

2.2.5. Segregation of the target particle region from the background and extraction of surface feature pattern

Here, we take a replica image of heavy meromyosin (HMM) as an example and show the actual process to crop

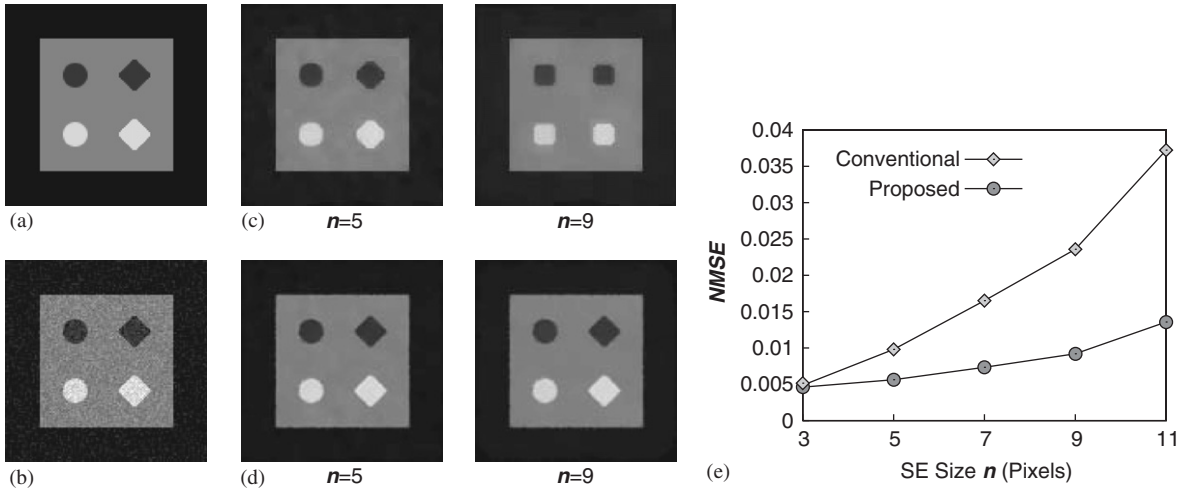

Fig. 3. Example of morphological smoothing. Comparison of the effect of smoothing between proposed and conventional methods. (a) Original image (123×123 pixels). The radius of a circle object in the internal area is 15 pixels, and the side length of the diamond in internal area is 15 pixels. (b) The same image but corrupted by random noise. (c) Smoothed images by conventional LOCO filter with square-shaped SE. (d) Smoothed images by proposed LOCO filter with square-shaped SE. (e) Artifacts due to filtering with various size of square-shaped SE.

the molecule region from the background. HMM (molecular weight about 350 kDa) consists of three portions; two globular subfragment-1s (S1, molecular weight about 110 kDa); whose carboxyl-terminals converge into rod-shaped subfragment-2 (S2) moiety. Each S1 consists of two regions, i.e. motor-domain (MD) and the lever-arm portion (LA). LA contains alpha-helical extension wrapped by two kinds of light chains called essential light chain (ELC) and regulatory light chain (RLC), respectively (Fig. 4(a)). Original replica image of HMM (Fig. 4(b)); details on the materials and methods are described in Ref. [16], was digitized at 0.1 nm/pixel in 8-bit gray-scale and was smoothed by the morphological filter. The target particle was segregated from the background by setting the appropriate threshold as above. Attention was paid to achieve the greatest performance concerning three points; always to keep the contrast between the region of target particle and background high enough, to keep the brightness within the region of the target particle as uniform as possible, and not to destroy the outline shape. Because the contrast of a replica EM image was very high, distinction between the region of the target particle and background was easy. However, areas with relatively low brightness were sometimes present within the region of the target particle. If binarization was carried out without appropriate smoothing, they could be regarded as "holes" in the middle of the target particle. Here, we used the LOCO filter based on rotational mathematical morphology in the smoothing process, to preserve the effectiveness of the proposed method. Fig. 4(b)–(j) shows one example of the proposed procedure to extract two S1 regions of single HMM independently. The original replica image (Fig. 4(b)) was first processed with a square-shaped SE of the adequate size, observing above cautions. The side-length of SE was set at 21 pixels (i.e. 2.1 nm). Fig. 4(c) represents the image after smoothing the relief narrower than 2 nm, indicating that the proposed method to give reasonable results. There, the foreground particle was well distinguished from the background while preserving the undulations in the contour shape of the particle, but the potential cavities within the molecule region were evenly filled. Fig. 4(d) shows the result after its binarization. The foreground particle was appropriately separated from the background at certain value determined by Otsu's method [37] which maximize the discriminant measure variable and enables us to select nonparametric and unbiased threshold automatically from the histogram. Then, the size of the area occupied by each isolated object was calculated. If the size of certain object was less than that pre-defined, such object was discarded either as simple photographic noise, salt deposit called "eutectic" of replica specimens or the S2 region, and the gray level of those area was converted to background intensity. Thus, S1s region of the target was extracted from the original image (Fig. 4(e)). Then, the original image was cropped by a mask (Fig. 4(e)) to give the protein area (Fig. 4(f)). Each S1 was separated at the hinge, the narrowest and branched position (marked by arrowhead in Fig. 4(f)), by setting the SE to the smallest size wider than the hinge. All the area smaller than this SE was eliminated by smoothing (Fig. 4(g)), because the Opening operation substituted the brightness of this region with the background level (i.e. 0). The head moiety of HMM was trimmed into each S1 (Fig. 4(i)) by a binarized mask (Fig. 4(h)).

The surface feature was extracted from S1 images, again by top-hat transform. Considering the spatial resolution of the sample, the surface feature pattern, possibly reflecting the subdomain arrangement was defined as a convex structure within 2 nm. Thus, the side-length of the square-shaped SE was set as 2 (nm) and the surface feature was extracted from the internal area of the particle, followed by linear contrast stretching (Fig. 4(j)). The hills and the grooves were expressed as bright and dark pattern, respectively. The parameter of the rotational morphology (N) was set at 36, in all smoothing processes.

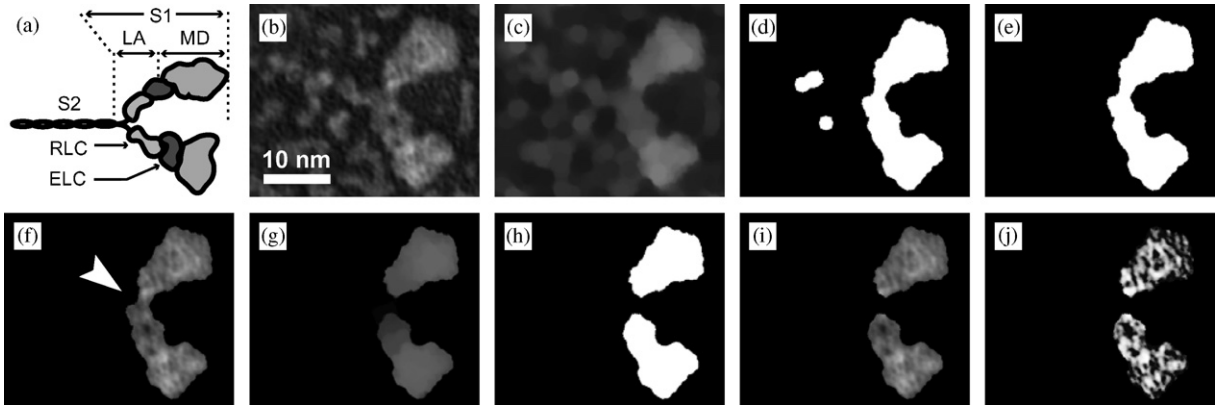

Fig. 4. Segregation of the target particle from background, and extraction of surface feature pattern from that region. (a) Schematic drawing of HMM composition. (b) Original replica image. (c) Smoothed image. (d) Binarized image of (c) with a threshold 77. (e) Mask to segregate molecule region. (f) Extracted S1 region. (g) Smoothed image of (f). (h) Binarized image of (g) with a threshold 49. (i) Finally cropped S1 target image. (j) Surface pattern extracted from the target.

2.3. Generation of template images and extraction of characteristic features

There are a number of theoretical considerations on the mechanism of image formation by rotary-shadowing [38–41]. Though it might be possible to simulate the rotary-shadowed replica images by strict application of above theoretics, it would apparently take great amount of computation time to generate a large number of template images we would need. Since the information requested for our purpose is simply the position of subdomains on the surface of the molecules, we took the advantage of much faster approach that satisfies the minimum requirement. Thus, we likened the images of metal shadowed molecules to the atomic models illuminated by surrounding lights, so that we could generate comprehensive set of artificial images most easily by using commercial ray-tracing software. Several studies correlated electron microscopic images of metal-shadowed samples to the images of the solid-model illuminated by the lighting source [42,43]. Though the physical process to form two kinds of images was apparently quite different from each other, preprocessing both of them with morphological filter enabled us to quantitatively compare the positions of hills and grooves by matching the image texture. More details on this crucial point will be discussed separately.

Atomic coordinates of the protein molecule were taken from the Protein Data-Bank (http://www.rcsb.org/pdb/index.html) for 3D model building, and a set of images representing the imaginary views of rotary-replicated molecules were produced utilizing light-rendering software adapted for this specific purpose ("Shade 6 professional Rev. 19", e-frontier, Inc. that was supplemented with homemade plug-in's). Each atom was expressed as 4 nm radius sphere with no specular reflection; i.e. ideal Lambert surface. The effect of rotary shadowing was replaced by virtual lighting of the atomic model from eight (maximum number as default) equally spaced light sources (Fig. 1(b)), surrounding the model. The orientation of the view-angle was implemented as the rotation of the model from the original co-ordinates by three angles (view angles; equivalent to Euler angles). Parameters ϕ, θ and ψ specify rotation angles around the x-, y- and z-axes; and the projection was made parallel to the z-axis, so that the change in ϕ and θ includes the movement along the line of sight, whereas the change in ψ represents a planar rotation. Actual rotation of the single conformer was carried out every 10° in solid angles to generate comprehensive set of template images. By this way, structural information of the molecular surface features like grooves, and hills were automatically implemented into projected images of the solid model and expressed as light and dark regions, respectively.

Correlation analysis is the standard method for the quantitative comparison among various images. The mandatory process to obtain reliable results is to match the texture of all the images in question as much as possible. Since the quality of artificial model-images apparently differed from that of true replica images, we once more utilized morphological filter for texture matching of two kinds of images of distinct entity. The feature patterns of the artificial images were extracted in a similar manner to that for target replica images. Those structural data were stored in the database for later comparison. The total number of templates stored in the database was about 15,000 for a single conformer.

2.4. Outline-based matching

The first step of the recognition process in the retrieval phase was the matching between the target particle image and templates based on the outline shape. Fourier descriptors or complex autoregressive models might be most frequently used to represent object's shapes. However, they request a priori information related to the ordering of the points along the outline curve. Since the calculation of the curvature requires the evaluation of second derivatives, difficulties would arise especially when the objects are small or noisy. Since we needed the descriptor sensitive to the rotation of the object, they were not appropriate for our present purpose. Peripheral feature is another descriptor originally proposed for character recognition [44]. It is a rotation variant which has been successfully applied to offline signature verification as an effective parameter to represent the outline shape of object [45]. We employed this feature to compare the outline shape and angle of planar rotation in between target particle and the templates.

The peripheral feature of the molecule was defined and processed as follows (Fig. 5(a)). Rectangular area circumscribing the whole molecule was taken and the brightness of the pixels in the molecule region and the background were set as 1 (white) and 0 (black), respectively. The long side length of that region was normalized to 256 pixels. Then the total area was expanded into 256×256 pixel-square while keeping its gravity center.

Then square-shaped binary image was subdivided into horizontal and vertical strips of single pixel-width. Within each strip, the length between the edge of the virtual frame and the first black-to-white pixel jump was calculated. This operation generates a $4 \times N_s$ peripheral feature vector (four edges with N_s strips for each edge, e.g. $N_s = 256$, in this study, for the full resolution). Let the feature vector be denoted by $\boldsymbol{v} = (v_1, v_2, \ldots, v_{4 \times Ns})^T$ where T stands for transpose.

The similarity of the peripheral feature vector between the target particle and the set of templates was measured as normalized cross-correlation coefficient. Let $\boldsymbol{v_p}$ define a peripheral feature vector of the target particle and $\boldsymbol{v_t}$ a peripheral feature vector of a template, both with dimension K. Normalized cross-correlation coefficient r_{os} was expressed by the formula

$$r_{os} = \frac{\sum_{i=1}^{K}(v_{pi} - \mu_p)(v_{ti} - \mu_t)}{\sqrt{\sum_{i=1}^{K}(v_{pi} - \mu_p)^2}\sqrt{\sum_{i=1}^{K}(v_{ti} - \mu_t)^2}}, \tag{10}$$

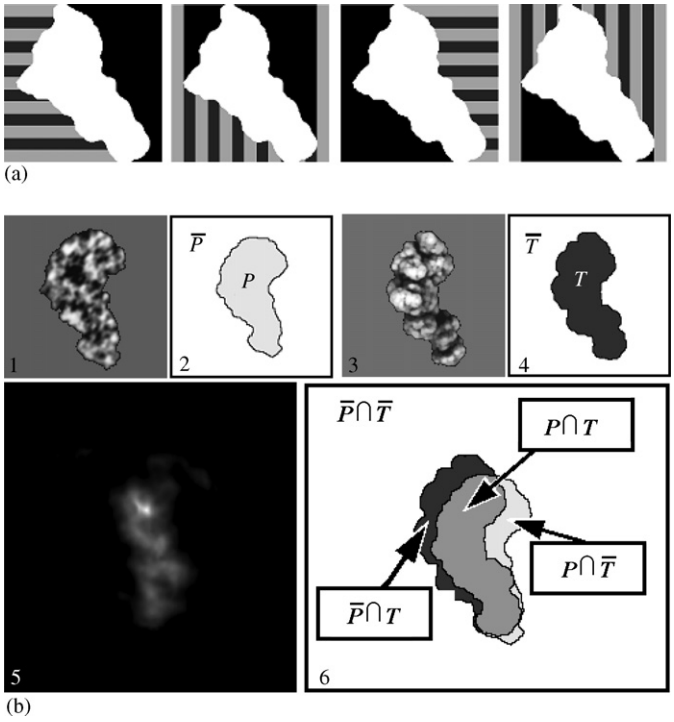

Fig. 5. (a) Extraction of peripheral feature. The area in the square but excluded by the molecule was sliced into strips along four sides, and the sequential length values of the strips were taken as the constituents of the feature vector. Altogether, a 1024-dimensional feature vector was extracted. (b) Surface pattern-based matching and the definition of fitness. (b1) Surface pattern of the target particle. (b2) Molecule region of the target. (b3) Surface pattern of the template. (b4) Molecule region of a template. (b5) Correlation map between the target and a template. Correlation coefficient was expressed as brightness level. In this search window, maximum brightness; 255 was assigned to maximum correlation coefficient. (b6) Spatial relationship of a molecule region of the target and a template. The ratio of overlapping area in the total area was defined as "fitness".

where $\mu_p = (1/K)\sum_{i=1}^{K} v_{pi}$ and $\mu_t = (1/K)\sum_{i=1}^{K} v_{ti}$. Here, dimension $K = 4 \times N_s$. r_{os} ranges from -1 to $+1$. Similarity of the outline shape was evaluated by this score and the templates with higher similarity were selected as the candidates to proceed to the next step.

2.5. Surface pattern-based matching and calculation of fitness score

In the second step, the surface pattern and the area of molecule region of selected templates were reloaded and compared with those of the target, one by one. Search window was created by the surface pattern image of the target particle, and its similarity with each template was estimated as normalized cross-correlation coefficient r_{sp}. The score, useful to find the degree of matching of a template $I_t(i,j)$ of size $m \times m'$ in a search window $I_p(i,j)$ of size $M \times M'$ was defined as

$$r_{sp} = \frac{\sum_{i=1}^{m}\sum_{j=1}^{m'}\{I_p(i,j) - \mu'_p\}\{I_t(i,j) - \mu'_t\}}{\sqrt{\sum_{i=1}^{m}\sum_{j=1}^{m'}\{I_p(i,j) - \mu'_p\}^2}\sqrt{\sum_{i=1}^{m}\sum_{j=1}^{m'}\{I_t(i,j) - \mu'_t\}^2}}, \tag{11}$$

where, $\mu'_p = (1/mm')\sum_{i=1}^{m}\sum_{j=1}^{m'} I_p(i,j)$ is the averaged gray level of corresponding part of the search window matrix, and $\mu'_t = (1/mm')\sum_{i=1}^{m}\sum_{j=1}^{m'} I_t(i,j)$ is the counterpart of the template matrix. (i,j) are the number of rows and columns of the template matrix. For all $(i,j) \in M \times M'$. r_{sp} ranges from -1 to $+1$.

However, the value of background area of target particle and template was replaced by the averaged gray level within the particle area.

Though cross-correlation function search is generally the method of choice to accurately classify the particles according to their projection angles, malclassification could sometimes happen. In fact, we often encountered the cases where the appearance of a template resembled to the other, though the actual projection angle was completely different from each other. This problem is inevitable, as long as only a single feature was used in the search of view-based system. So, we introduced the fitness score that evaluates the degree of overlapping of a molecule region of the target particle and the template, and it was further integrated with a similarity of a surface feature pattern. The fitness was defined as follows (Fig. 5(b)). The molecule region of the target particle in the search window and an excluded region were expressed by the signs P and $\bar{P}$ (Fig. 5(b2)), respectively. The region occupied by the molecule and the excluded region for the template were expressed by the signs T and $\bar{T}$ (Fig. 5(b4)), respectively. Then the fitness was

$$\text{Fitness} = 1 - \frac{(\bar{P} \cap T) \cup (P \cap \bar{T})}{P}. \tag{12}$$

When matching procedure was finished, the fitness at the point should be unity if following conditions were satisfied.

$$\bar{P} \cap T = 0, \tag{13}$$

$$P \cap \bar{T} = 0. \tag{14}$$

Condition (13) means that a molecule region of a template must not protrude from a molecule region of the target particle. Condition (14) defines that all of a molecule region of target being covered by a molecule region of a template. Figs. 5(b1) and (b2) exhibit the example of surface pattern of the target particle and the one within the molecule region. Fig. 5(b3) shows one of the templates, and Fig. 5(b4), its image in the molecule region. A template window was shifted pixel by pixel across a larger search window, and in each position, the cross-correlation coefficient r_{sp} between the template window and the corresponding part of the search window was computed according to Eq. (11). Then, the fitness was calculated at the position where maximum cross correlation coefficient (r_{sp_max}) was obtained. Fig. 5(b5) indicates the map of correlation coefficient between a search window created by the target particle (Fig. 5(b1)) and a template (Fig. 5(b3)). The actual overlap of two molecule regions at the best-matching position is shown in Fig. 5(b6). For similarity retrieval of the target, each template was rated

according to the value of fitness and the template with a maximum fitness was selected as the best-matching candidate for the view-angle of the target.

2.6. Determination of the conformational type of target particle

Further attempt was made to determine the most likely conformation of the target particle. The best candidate was selected from each database generated for all available conformers. Since they were determined according to the fitness, the outline shape and the size of the selected templates should be similar to the target particle. On the other hand, the fitting of the surface pattern to that outline is an independent matter and should be evaluated separately for more effective discrimination. According to this idea, we employed a norm of the fitness and the correlation coefficient of the surface pattern, as an index for the judgment of the configuration. This coefficient r_{conf} was defined as follows.

$$r_{\mathrm{conf}} = \sqrt{(r_{\mathrm{sp\_max}})^2 + (\mathrm{Fitness})^2}, \tag{15}$$

where, r_{conf} is defined in $r_{\mathrm{sp\_max}} \geqslant 0$ and $\mathrm{Fitness} \geqslant 0$. r_{conf} ranges from 0 to the maximum $\sqrt{2}$ when $r_{\mathrm{sp\_max}}$ and Fitness are equal to unity.

3. Application and evaluation of proposed procedure

We applied the proposed method to quick-freeze deep-etch replica images of HMM heads in putative transition state as stabilized by simultaneous binding of ADP and inorganic vanadate. Since the structure of such complex has been well characterized both by X-ray crystallography [46] and EM [16], it might give a good measure to examine the feasibility of the novel procedure. Some of the original images of sampled particles (Fig. 6(a)) [16] indicate characteristic strongly kinked configuration as reported, but the others (numbered 4, 6 and 8) not. The second row (Fig. 6(b)) shows the surface patterns extracted from respective images. Now, we will pick up the first particle (Fig. 6(a1)) as an example and show the typical flow along the actual application procedure. At first, a comprehensive set of template images were generated with an angular step of 10° from the atomic coordinates of the scallop myosin S1 that was downloaded from the Protein Data-Bank (ID:1DFL). Then, the characteristic features were extracted from each image and stored for later comparison with the target image. Next, similar features were extracted from the target image and were subjected to the examination. Fig. 7(a) shows the result of similarity retrieval by the outline-based matching. Templates were rated according to

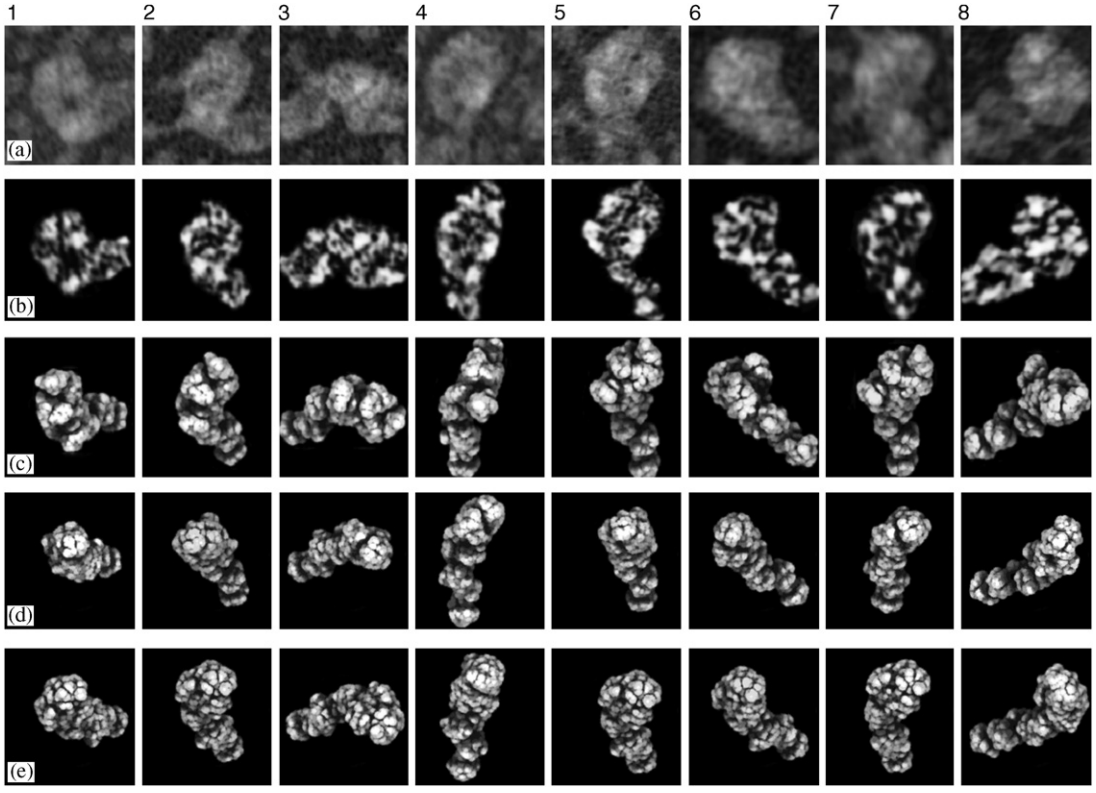

Fig. 6. Electron microscopic images of quick-freeze deep-etch replica of heavy meromyosin in ADP/inorganic vanadate transition state, and the best-matched templates for each configuration as determined by the present procedure. Only one of two heads for each molecule is indicated. (a) Original images. (b) Extracted surface pattern of the target particles. (c–e) Best-matched templates for three crystallographic configurations. (c) Vanadate-transition state (d) Near-rigor state. (e) ADP state. According to the computer analysis, the right conformation was the vanadate-type for all of them and the Euler angles of these templates were; no. 1: (14, 23, 6), no. 2: (3, 23, −54), no. 3: (−13, 13, −134), no. 4: (−56, 27, −59), no. 5: (8, −7, −64), no. 6: (−121, 7, −19), no. 7: (−7, 3, −74), no. 8: (43, −15, −161).

the similarity to the target particle. Maximum distance was calculated from maximum and minimum value of a similarity and the normalized distance (ND) was defined as the difference between them.

$$\mathrm{ND} = (\mathrm{max\_value}) - (\mathrm{min\_value}). \quad (16)$$

Tentative first-stage candidates were selected from the templates in the database that had less than top 10% threshold value of ND. In this case, 46 templates with a similarity score higher than threshold (= 0.84) survived. Then, the candidates were subjected to the second-stage retrieval by the similarity of surface pattern-based matching. ND was calculated in the same way as before to set the adequate threshold for the final selection. Fig. 7(b) shows the distribution of view angles of the templates qualified to have less than 5% ($ND_{0–5\%}$), 5%–10% ($ND_{5–10\%}$),

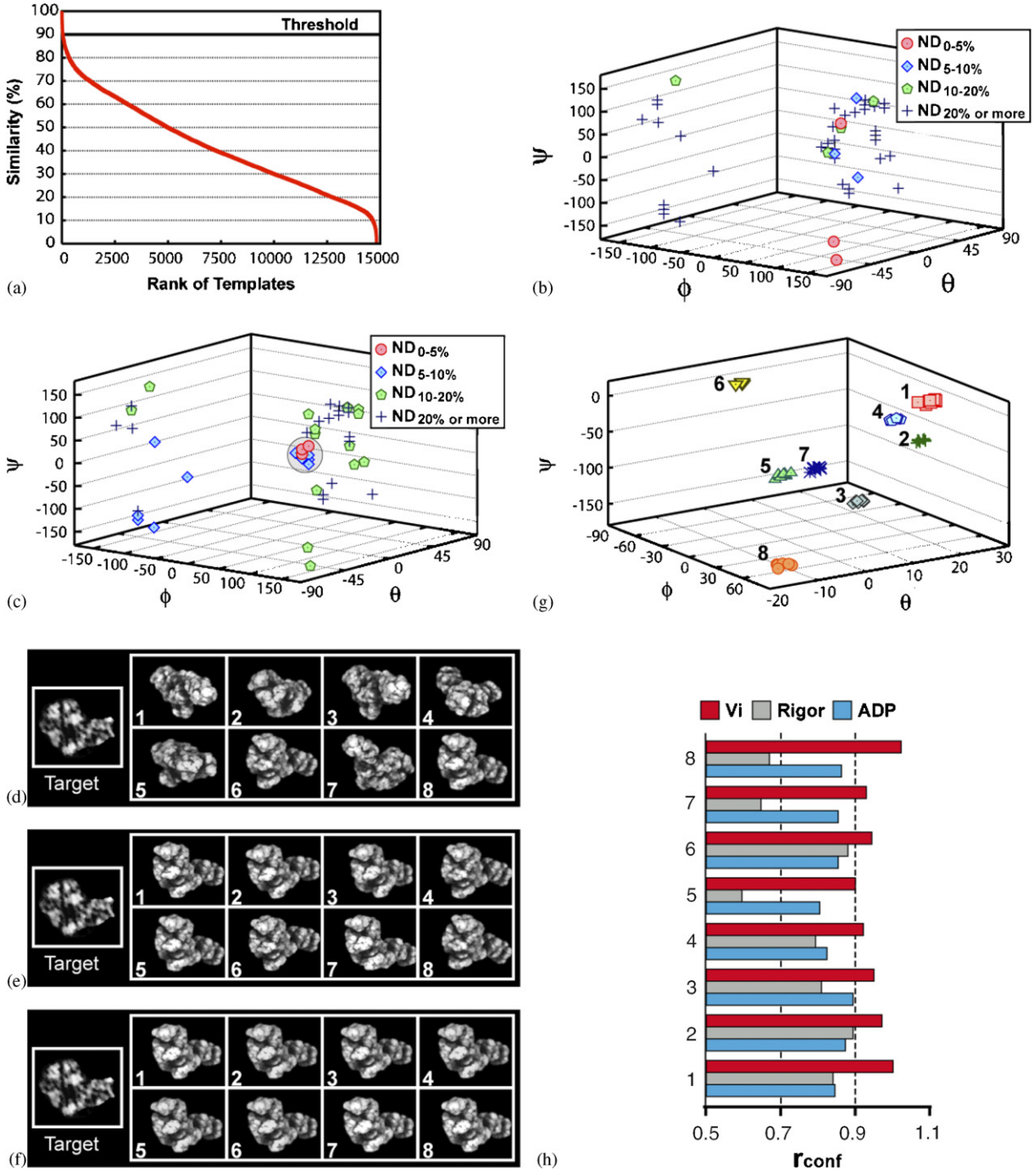

Fig. 7. Example of the results obtained in each step of our procedure. See text for the details. (a) Ranking of the templates according to outline-based matching for target particle No. 1. ND measured in r_{os} is shown in a vertical axis. (b, d) Distribution of view angles of the templates selected by matching of the surface pattern for no. 1 particle. (c, e) Distribution of view angles by surface pattern-based matching combined with the fitness. (f) Finally selected templates by finer search. (g) Distribution of view angles of eight samples in Fig. 6(a). (h) Discrimination of the conformational type by r_{conf}.

10%–20% ($ND_{10–20\%}$), and 20% or more ($ND_{20\% \text{ or more}}$) of ND. We first expected that the view-angles corresponding to highly scored templates would distribute within the narrow range of projection angles, naturally because the close view direction should give the analogous appearance of the object. However, the selected angles were rather randomly scattered and, at first, we could not grasp the reason for such consequence. Fig. 7(d) shows the actual template images that were rated as the top 8. The appearance of the top-ranked candidates differed greatly from each other and we could not recognize the similarity among them, at a glance. We further sought for the reason for the false similarity and found that the erroneous results might be attributable mainly to the presence of highly contrasted region that matched locally. This is exactly the reason why we introduced the new parameter "fitness". We reexamined the performance of the above procedure after that improvement, it is notable that, this time, the templates having higher similarity (less than 10% of total) to the target particle formed a clear cluster; indicated by gray hatching (Fig. 7(c)), justifying the final selection being highly likely.

Though cluster-formation might be considered as a natural consequence of the closeness in the projection angle in space, it turned out to be a good measure for the consistency of the selection. Thus, the reliability for the final decision dramatically improved by the combination of surface pattern matching and the fitness scoring.

After confirming the consistency of the approximate view-angles of templates by clustering, finer search was carried out for more precise determination of the projection angle around the cluster (Fig. 7(c)). Templates were prepared with 1° angular increment within a range of $\pm 20^\circ$ of the best-matched candidate in the preceding selection. Fig. 7(f) exhibits final top 8 templates and it is obvious that that we might reach very accurate results while saving the computation time, by the use of coarse-to-fine matching method.

We applied the same procedure to determine the projection angle of the other particles (Fig. 6(a)) that were picked up from the same replica specimens. Fig. 7(g) shows the projection angles for eight particles with various projection angles (Fig. 6(a)) all clustered around the most likely view for each target. The gallery of best-matched templates is exhibited in Fig. 6(c).

Analogous search was conducted to define the best-matching conformation of the target. Scallop myosin S1 is the only species whose crystallographic structures with various nucleotides were systematically determined as in different configurations. We took three structures; i.e. near-rigor state (1DFK) and ADP state (1B7T) and vanadate-transition state (1DFL), from the data-base and archived their templates. Figs. 6(d) and (e) exhibit the best-rated candidates for Rigor and ADP-type templates according to the fitness. Norm scores were distinctively high when template's configuration matched with the true structure of the target (Fig. 7(h)). Among 72 target particles examined, the mean $\pm$ SD (standard deviation) of r_{conf} for various conformations were as follows: 0.95 ± 0.048 for Vi/Vi was, 0.73 ± 0.098 for Vi/Rigor and 0.74 ± 0.089 for Vi/ADP. Thus, all the samples were correctly determined as to be in vanadate-transition state. Preliminary attempts with the other replica images containing different conformers confirmed the reliability of the final judgment by our procedure. Thus, our novel methodology enables a correct determination of two structural information; the configuration and the view angle of the particles observed in quick-freeze replica images.

4. Discussion

4.1. Difference in the texture of replica and model images and the crucial role of morphology filter

We conveniently utilized commercial light-rendering software to generate a huge number of templates from the atomic models of the protein assembly, and succeeded to identify the best- matching candidates corresponding to given replica images. Though both processes might bear nominally common process "shadow-formation", it is apparent that they cannot be related in a straightforward manner, since physical process of image formation is quite different from each other. Rotary-shadowed replica specimens are prepared in dedicated vacuum-apparatus and are observed under transmission electron microscope. As a result of heavy-metal evaporation from certain elevation angle, the thickness of the metal coat on the surface of the target particle, Δ, changes according to the incident angle Θ of the metal beam from the gun. This is expressed as $\Delta = \Delta_0 \cos \Theta$ [47] where, Δ_0 is the maximum thickness obtained for $\Theta = 0$. The observed density at given point of the replica specimen depends on the path length along the transmission electron beam. Since the image contrast comes from the differential density of the point from the surrounding area, the grooves flanked by two opposing slopes of large subdomain hills give high contrast line profile along globally globular surface of the molecular architecture. Next, suppose that we have the atomic model of the target protein assembly, which is illuminated from surrounding light sources. If the size of the atom is tactically set so that subdomain structures appear as clusters of spherical atoms that closely overlap to make globally globular structure, we would be able to generate the model image, in which only the thicker grooves between large clusters appear dark enough to be caught by human eye, while the finer ones do not. When such images were adequately smoothed, only the large globular subdomains surrounded by relatively thick grooves would become prominent exhibiting characteristic subdomain arrangement separated by dark streak pattern on the surface of the atomic model. Thus, the position of the tops of the hills and the grooves in between would nicely match with those observed in replica images. However, there are definitely some differences in the image properties because

of the different physical processes that might hamper their straightforward comparison. For instance, rotary-shadowed particles under transmission EM appear very bright at the edges of the target because of the long electron path along the standing metal coat. Though the surface pattern of extreme edge is impossible to evaluate, structural information along the edge is included as overall peripheral shape. On the other hand, the delicate pattern of hills and grooves in the major area of the molecule could easily be picked up for comparison with artificial surface image of the model. Since the filter we devised can effectively enhance the features of predetermined shape and scale, global difference of the texture of two kinds of images were effectively cancelled, enabling us to examine the precise positions of surface features.

4.2. Robustness of our procedure against various perturbations

Though the replica specimen by itself gives high-contrast low-noise images, there are still remaining sources to deteriorate the quality of the final target images. They are salt and pepper noise or slight blurring in some of the images, which are almost unavoidable during photographic procedure, because we need extremely high-magnification view of the target particles picked up from the original negatives that had been already taken with very high direct magnification. To evaluate the robustness of our method against various perturbations, we examined how the background noise affects the final decision by the computer. Instead of real target images, we employed artificial model images to which two kinds of perturbations were added to various extents. Actually, six model images were prepared as target, a control (T_0, T_{e0} and T_{g0}, in Fig. 8) and five others by addition of random noise plus Gaussian blur (T_1–T_5, T_{e1}–T_{e5} and T_{g1}–T_{g5}). Effects of perturbations were examined at first for view-angle determination. Templates were prepared by rotation of the atomic model with 5-degree increment around y-axis from the original position ($-180^\circ \leqslant \theta \leqslant 180^\circ$). Fitness was scored for each template to find the best-matching one (Fig. 8(a) and enlarged view of its central part). Though the absolute fitness score declined according to the noise level, the final answer to the best-matching angle remained the same.

The validity of conformational search was assessed in a similar manner but assuming the different views of the same target structure (Vi-type) showing two extreme appearances (“extended”, T_e and “globular”, T_g, in Fig. 8(b)). Again substantial level of perturbation intentionally added to the target image did not affect the ranking of the likely conformation, further confirming the robustness of our procedure.

4.3. Upcoming application of our procedure to the other materials and occasions

In this paper, we proposed a novel template-matching method to determine the view angle of protein image observed by a quick-freeze deep-etch replica EM. Its practical utility was confirmed with the images of myosin

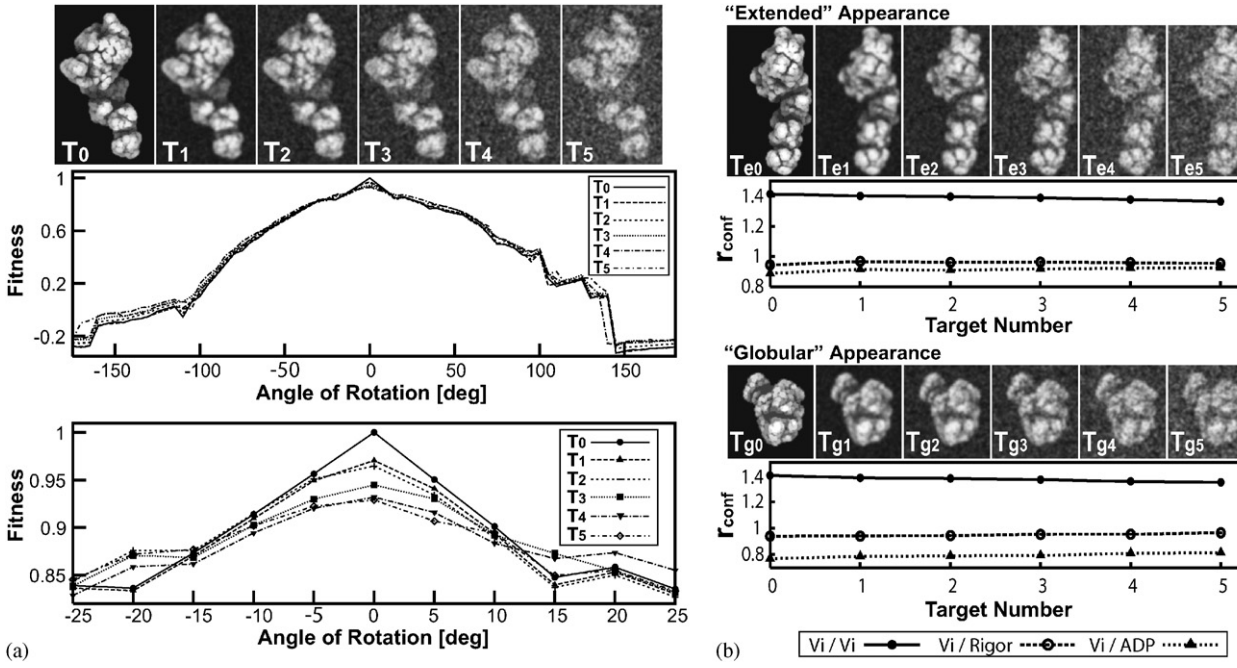

Fig. 8. Influence of added noise to final recognition of view-angle and conformational state. An artificial image of Vi-type structure was used as a target. (a) Fitness scores when target image was deteriorated by the addition of noise, so that peak signal-to-noise ratio (PSNR) became T_1: 26.62 [dB], T_2: 21.61 [dB], T_3: 18.38 [dB], T_4: 15.94 [dB], and T_5: 14.10 [dB], respectively. (b) Norm scores (r_{conf}) of two different views when target was deteriorated so that PSNR reduced to T_{e1}: 26.39 [dB], T_{e2}: 21.57 [dB], T_{e3}: 18.33 [dB], T_{e4}: 15.88 [dB], T_{e5}: 14.14 [dB], and PSNR by degradation of T_{g0}; T_{g1}: 27.13 [dB], T_{g2}: 21.67 [dB], T_{g3}: 18.32 [dB], T_{g4}: 15.67 [dB], T_{g5}: 13.92 [dB].

heads as test-materials. A great advantage of our procedure is that even a single view of the target particle can be the subject of analysis.

Though template-matching is a common procedure widely used in various fields of technology, its use in EM seems to be rather limited. During the course of 3D image-reconstruction of the live cells by a tomographic approach, Baumeister's team attempted to automatically classify the species of macromolecular assemblies that co-existed, by template-matching [48,49]. There, the target and the templates were both 3D structures reconstructed either by tomography or single-particle analysis, and its practical application to general objects might not be as easy as in our procedure dealing with 2D images. As a matter of fact, we imagine that the extraction of the characteristic features of the target and template particles according to our procedure might work effectively, even in their studies.

Since quick-freeze deep-etch replication can equally visualize the instantaneous structure of protein assemblies in solution or in live cells [50,51], the proposed image analysis procedure should be generally applicable to determine the surface features of various protein assemblies there. Such structural information might be a fruitful source to give us a hint of unknown molecular mechanisms of various biological events. Current procedure worked almost perfectly, when the target particles were well isolated from the others, but may not be so where two or more particles intimately collide to form tightly fused images. We are currently upgrading the algorithm so that sufficiently reliable structure can be available even if a part of the total structure is occluded by the interaction with the other components. We expect that our procedure would find even larger field of applicability after such improvement.

5. Conclusion

We proposed a procedure to define the delicate surface pattern of the protein molecules captured by quick-freeze deep-etch replica EM. We applied the procedure to the replica image of HMM heads as test-materials. The system successfully recognized the most likely projection angle and the conformation of the sampled particles. In future, we might directly analyze the gross structure of macromolecular assembly captured under functional states, wishfully even in live cells in situ.

Acknowledgments

We thank Dr M. Fujio for his kind reading and comments on the manuscript and to Ms. T. Shiraishi for her expert technical assistance especially in replica preparation and photography. We are greatly indebted to Dr. T. Kodama for his warm encouragement and useful advice on this study. This work was partly supported by Grants-in-Aid for Scientific Research B and Grants-in-Aid for Specific Areas to E.K. from the Ministry of Education, Culture, Sports, Science and Technology of Japan. This work was also supported by Technology Development Program for Advanced Measurement and Analysis (Program-T) from Japan Science and Technology Agency to E.K.

References

[1] Y. Harada, T. Funatsu, M. Tokunaga, K. Saito, H. Higuchi, Y. Ishii, T. Yanagida, Methods Cell. Biol. 55 (1998) 117.
[2] A. Abbott, Nature 417 (2002) 894.
[3] J. Frank, J. Zhu, P. Penczek, Y. Li, S. Srivastava, A. Verschoor, M. Radermacher, R. Grassucci, R.K. Lata, R.K. Agrawal, Nature 376 (1995) 441.
[4] J. Frank, P. Penczek, R.K. Agrawal, R.A. Grassucci, A.B. Heagle, Methods Enzymol. 317 (2000) 276.
[5] I.S. Gabashvili, R.K. Agrawal, C.M.T. Spahn, R.A. Grassucci, D.I. Svergun, J. Frank, P. Pnczek, Cell 100 (2000) 537.
[6] M. van Heel, B. Gowen, R. Matadeen, E.V. Orlova, R. Finn, T. Pape, D. Cohen, H. Stark, R. Schmidt, M. Schatz, A. Patwardhan, Q. Rev. Biophys. 33 (2000) 307.
[7] T. Ogura, C. Sato, J. Struct. Biol. 136 (2001) 227.
[8] K. Mio, T. Ogura, Y. Hara, Y. Mori, C. Sato, Biochem. Biophys. Res. Commun. 333 (2005) 768.
[9] C.W. Taylor, P.C.A. da Fonseca, E.P. Morris, Trends Biochem. Sci. 29 (2004) 210.
[10] J.E. Heuser, J. Mol. Biol. 169 (1983) 155.
[11] J. Usukura, Y. Nishizawa, A. Shimomura, K. Kobayashi, T. Nagatsu, M. Hagiwara, Genes Cells 5 (2000) 515.
[12] W. Colquhoun, R. Sokol, J. Electron. Microsc. Tech. 3 (1986) 169.
[13] S. Eskandari, M. Kreman, M.P. Kavanaugh, E.M. Wright, G.A. Zampighi, Proc. Natl. Acad. Sci. USA 97 (2000) 8641.
[14] T. Walz, P. Tittmann, K.H. Fuchs, D.J. Müller, B.L. Smith, P. Agre, H. Gross, A. Engel, J. Mol. Biol. 264 (1996) 907.
[15] H. Winkler, H. Gross, Scanning Microsc. Suppl. 2 (1988) 379.
[16] E. Katayama, J. Mol. Biol. 278 (1998) 349.
[17] E. Katayama, N. Ichise, N. Yaeguchi, T. Yoshizawa, S. Maruta, N. Baba, Adv. Exp. Med. Biol. 538 (2003) 295.
[18] J. Serra, Image Analysis and Mathematical Morphology, Academic Press, London, 1982.
[19] R.M. Haralick, S.R. Sternberg, X. Zhuang, IEEE Trans. Pattern Anal. Mach. Intell. 9 (1987) 532.
[20] C.R. Giardina, E.R. Dougherty, Morphological Methods in Image and Signal Processing, Prentice-Hall, Englewood Cliffs, NJ, 1988.
[21] P. Maragos, R.W. Schafer, IEEE Trans. Acoust. Speech Signal Process. 35 (1987) 1153.
[22] P. Maragos, R.W. Schafer, IEEE Trans. Acoust. Speech Signal Process. 35 (1987) 1170.
[23] P. Maragos, R.W. Schafer, Proc. IEEE 78 (1990) 690.
[24] J. Serra, Comp. Vision Graph. Image Process. 35 (1986) 283.
[25] S.R. Sternberg, Comp. Vis. Graph. Image Process. 35 (1986) 333.
[26] P.S. Adiga, R. Malladi, W. Baxter, R.M. Glaeser, J. Struct. Biol. 145 (2004) 142.
[27] A.S. Frangakis, R. Hegerl, J. Struct. Biol. 138 (2002) 105.
[28] R.A. Peters, IEEE Trans. Image Process. 4 (1995) 554.
[29] R.L. Stevenson, G.R. Arce, IEEE Trans. Circuits Syst. 34 (1987) 1292.
[30] D. Schonfeld, J. Goutsias, IEEE Trans. Pattern Anal. Mac. Intell. 13 (1991) 14.
[31] M.A. Schulze, J.A. Pearce, in: Proceedings of the IEEE International conf. Acoust. Speech Signal Process, 1993, Vol. 5, p. 57.
[32] S.C. Pei, C.L. Lai, F.Y. Shih, Pattern Recogn. 31 (1998) 1127.
[33] F.Y. Shih, Y.T. Wu, Pattern Recogn. 37 (2004) 79.
[34] J. Song, E.J. Delp, Comp. Vis. Graph. Image Process. 50 (1990) 308.
[35] H. Kobatake, Y. Yoshinaga, IEEE Trans. Med. Imaging 15 (1996) 235.

[36] F. Meyer, Contrast feature extraction, in: J.-L. Chermant (Ed.), Quantitative Analysis of A Microstructures in Material Sciences, Biology and Medicine, Special Issue of Practical Metallography, Riederer Verlag, Stuttgart, 1978, p. 374.
[37] N. Otsu, IEEE Trans. Syst. Man Cybern. 9 (1979) 62.
[38] P.R. Smith, J. Kistler, J. Ultrastruct. Res. 61 (1977) 124.
[39] L. Landman, J. Roth, J. Microsc. 139 (1985) 221.
[40] J.P. Chalcroft, Ultramicroscopy 16 (1985) 371.
[41] R. Guckenberger, Ultramicroscopy 16 (1985) 357.
[42] V.D. Vasiliev, O.M. Selivanova, S.N. Ryazantsev, J. Mol. Biol. 171 (1983) 561.
[43] B. Tesche, H. Schmiady, Ultramicroscopy 16 (1985) 423.
[44] M. Umeda, IEICE Trans. Inf. syst. E 79D (1996) 401.
[45] B. Fang, C.H. Leung, Y.Y. Tang, P.C.K. Kwok, K.W. Tse, Y.K. Wong, IEE Proc. Vis. Image Signal Process. 149 (2002) 85.
[46] C.A. Smith, I. Rayment, Biochemistry 35 (1996) 5404.
[47] R. Krbecek, C. Gebhardt, H. Gruler, E. Sackmann, Biochim. Biophys. Acta 554 (1979) 1.
[48] J. Walz, D. Typke, M. Nitsch, A.J. Koster, R. Hegerl, W. Baumeister, J. Struct. Biol. 120 (1997) 387.
[49] J. Böhm, A.S. Frangakis, R. Hegerl, S. Nickell, D. Typke, W. Baumeister, Proc. Natl. Acad. Sci. USA 97 (2000) 14245.
[50] E. Katayama, H. Funahashi, T. Michikawa, T. Shiraishi, T. Ikemoto, M. Iino, K. Mikoshiba, EMBO J. 15 (1996) 4844.
[51] E. Katayama, T. Shiraishi, K. Oosawa, N. Baba, S.-I. Aizawa, J. Mol. Biol. 255 (1996) 458.